HHS Public Access

Author manuscript

Curr Biol. Author manuscript; available in PMC 2021 March 09.

Published in final edited form as:

Curr Biol. 2020 March 09; 30(5): 767–778.e5. doi:10.1016/j.cub.2019.12.049.

Tropomodulins Control the Balance between Protrusive and Contractile Structures by Stabilizing Actin-Tropomyosin Filaments

Reena Kumari[1], **Yaming Jiu**[1,6,7], **Peter J. Carman**[2,3], **Sari Tojkander**[4], **Konstantin Kogan**[1], **Markku Varjosalo**[1], **Peter W. Gunning**[5], **Roberto Dominguez**[2], **Pekka Lappalainen**[1,8,*]

[1]HiLIFE Institute of Biotechnology, University of Helsinki, PO Box 56, 00014 Helsinki, Finland [2]Department of Physiology, Perelman School of Medicine, University of Pennsylvania, 728 Clinical Research Bldg, 415 Curie Boulevard, Philadelphia, PA 19104, USA [3]Graduate Group in Biochemistry and Molecular Biophysics, Perelman School of Medicine, University of Pennsylvania, Philadelphia, PA 19104, USA [4]Department of Veterinary Biosciences, Faculty of Veterinary Medicine, University of Helsinki, Agnes Sjöberginkatu 2, 00014 Helsinki, Finland [5]School of Medical Sciences, UNSW, Sydney, Wallace Wurth Building, Sydney, NSW 2052, Australia [6]CAS Key Laboratory of Molecular Virology and Immunology, Institute Pasteur of Shanghai, Chinese Academy of Sciences, Life Science Research Building 320, Yueyang Road, Xuhui District, 200031 Shanghai, China [7]University of Chinese Academy of Sciences, Yuquan Road No.19(A), Shijingshan District, 100049 Beijing, China [8]Lead Contact

SUMMARY

Eukaryotic cells have diverse protrusive and contractile actin filament structures, which compete with one another for a limited pool of actin monomers. Numerous actin-binding proteins regulate the dynamics of actin structures, including tropomodulins (Tmods), which cap the pointed end of actin filaments. In striated muscles, Tmods prevent actin filaments from overgrowing, whereas in non-muscle cells, their function has remained elusive. Here, we identify two Tmod isoforms, Tmod1 and Tmod3, as key compo- nents of contractile stress fibers in non-muscle cells. Individually, Tmod1 and Tmod3 can compensate for one another, but their simultaneous depletion results in disassembly of actin-tropomyosin filaments, loss of force-generating stress fibers, and severe defects in cell morphology. Knockout-rescue experiments reveal that Tmod's interaction with tropomyosin is essential for its role in the stabilization of actin-tropo- myosin filaments in cells. Thus, in contrast to their role in muscle myofibrils, in non-muscle cells, Tmods bind actin-tropomyosin filaments to protect them from depolymerizing, not elongating. Furthermore, loss of Tmods shifts the balance from linear actin-tropomyosin filaments to Arp2/3 complex-nucleated branched networks, and this phenotype can be partially rescued by inhibiting the Arp2/3 complex.

*Correspondence: pekka.lappalainen@helsinki.fi.

AUTHOR CONTRIBUTIONS

R.K., Y.J., R.D., and P.L. designed the study. Y.J. performed BioID screening and generated Tmod3 knockout cell line. P.J.C. carried out protein purification and pointed-end capping assays and analyzed the data. S.T. provided traction force dishes and performed data analysis. K.K. and R.K. analyzed the sequencing data. M.V. performed the BioID analysis. P.W.G. provided the tropomyosin antibodies. R.K. performed all the remaining experiments, data analysis, and data interpretation. R.K. and P.L. wrote the manuscript, with input from all other authors.

Collectively, the data reveal that Tmods are essential for the maintenance of contractile actomyosin bundles and that Tmod-dependent capping of actin-tropomyosin filaments is critical for the regulation of actin homeostasis in non-muscle cells.

INTRODUCTION

Actin filaments assemble into diverse three-dimensional structures that produce force for various vital processes in cells. These structures include branched actin networks in lamellipodia, which polymerize against the plasma membrane to push the leading edge forward during cell migration. Similar branched actin filament networks also provide force for the generation of plasma membrane invaginations during endocytosis. Actin filaments, together with myosin II filaments, also assemble into contractile structures, where the force is produced by ATP- dependent sliding of bipolar myosin II filaments along the anti- parallel array of actin filaments [1, 2]. In order to generate these and other functionally distinct actin filament arrays, different actin filament nucleation machineries have evolved. These include the Arp2/3 complex, which nucleates new actin filaments from the sides of pre-existing “mother filaments” to generate branched actin filament networks that are predominant at the leading edge of motile cells and in the sites of endocytosis. The other major class of actin nucleators is the formins family of proteins that binds to filament barbed ends to assemble linear arrays of actin filaments that are needed in the contractile actomyosin structures [3, 4].

The protein compositions and dynamic properties of distinct actin filament arrays are markedly different. The Arp2/3-complex-nucleated, branched actin networks display rapid turnover, and proteins that drive rapid actin filament turnover are enriched in these structures [5, 6]. On the other hand, formin-nucleated actin filament arrays are decorated by tropomyosins (Tpm), which stabilize actin filaments and recruit myosins to these structures [7, 8]. Importantly, recent studies showed that different actin assembly factors compete with each other for a limited pool of assembly-competent actin monomers in cells [9, 10]. Consequently, depletion of profilin, a small actin monomer-binding protein that delivers actin monomers to formins and Ena/VASP, results in an excessive assembly of Arp2/3-complex-nucleated actin structures at the expense of formin- and Ena/VASP-assembled actin filament arrays [11, 12]. Thus, a fine balance in actin filament nucleation exists between Arp2/3 complex, formins, as well as Ena/VASP actin-polymerizing proteins.

Compared to protrusive actin filament arrays, the actin filaments in contractile actomyosin structures, such as muscle myo- fibrils and the stress fibers of non-muscle cells, undergo slower turnover [13–15]. Both myofibrils and stress fibers are composed of a bipolar array of myosin II and Tpm-decorated actin filaments. Although myofibrils contribute exclusively to muscle contraction, stress fibers are involved in diverse processes, including cell migration, adhesion, morphogenesis, and mechanosensing [16]. Actin filaments in myofibrils are stabilized by CapZ and tropomodulins (Tmods), which cap the barbed and pointed ends of sarco- meric actin filaments, respectively [17]. However, the mechanisms regulating the turnover of actin filaments in stress fibers of non- muscle cells are less well understood.

Tmods interact with the pointed end of an actin filament through their two actin-binding sites. In addition, Tmods contain two Tpm-binding sites, and thus, they bind tropomyosin-deco- rated filaments with higher affinity (K_d $20 nM) compared to bare actin filaments (K_d $0.1–0.2 mM) [18, 19]. Mammals have four Tmod isoforms, Tmod1, expressed in various post-mitotic cells; Tmod2, expressed in neurons; Tmod3, expressed ubiquitously in different tissues; and Tmod4, mainly in skeletal muscles [20]. All Tmod isoforms cap actin filament pointed ends, but Tmod3 can also bind actin monomers [21]. Genetic studies demonstrated that deletion of the two most widely expressed isoforms, Tmod1 and Tmod3, results in embryonic lethality in mice [22, 23].

The functions of Tmods have been thoroughly studied in stri- ated muscles, where they localize to the pointed ends of sarcomeric actin filaments. Inactivation of Tmods in fully developed striated muscles results in an increase in the length of thin filaments, although the overexpression resulted in shorter filaments, indicating that they function as negative regulators of actin filament elongation [13, 24–26]. Similar to striated muscles, Tmods control the regular length of actin filaments in the red blood cell mem- brane skeleton [27]. On the other hand, the functions of Tmods in other non-muscle cells are less well understood, and whether they prevent actin filaments from overgrowth, stabilize actin filaments, or control their organization has remained elusive. Tmods have been linked to exocytosis [28], assembly of cytoplasmic F-actin network in oocytes [29], as well as maintenance of the actin filament network at adherens junctions [30]. Tmod3 also contributes to cell migration and lamellipodia formation, with its depletion resulting in faster cell migration and its overexpression in decreased cell motility in endothelial cells [31]. However, whether Tmod3 functions as a negative regulator of cell migration by sequestering actin monomers, capping the pointed ends of lamellipodial actin filaments, or by some other mechanism is unknown. A recent study also revealed that a GFP-fusion of Tmod3 localizes to the stress fibers in a periodic pattern, similarly to the localization of Tmods in muscle myofibrils [32]. It is un- known, however, whether endogenous Tmods also localize to stress fibers and whether they contribute to stress fiber assembly, maintenance, and contractility.

Here, we examined the role of Tmods in human osteosarcoma (U2OS) cells. We reveal that Tmod1 and Tmod3 are critical for the maintenance of Tpm-decorated actin filaments in contractile actin stress fibers, and hence, simultaneous depletion of both isoforms led to a loss of stress fibers and drastic defects in cellular force production. We further show that stabilization of Tpm-decorated actin filaments by Tmods is critical for maintaining the balance between contractile actomyosin structures and Arp2/3-complex-nucleated branched actin filament networks in non-muscle cells.

RESULTS

Tmod1 and Tmod3 Are Components of Contractile Actin Stress Fibers

To identify novel stress fiber components, we performed a proximity-dependent biotin identification (BioID) analysis on human U2OS osteosarcoma cells by using a core stress fiber component, tropomyosin-3.1 (Tpm3.1), as a bait. With this approach, we identified pointed end-capping protein Tmod3 among the most abundant Tpm3.1-interaction partners (Table S1). Western blot and immunofluorescence microscopy analyses revealed that, in

addition to Tmod3, also Tmod1 is expressed in U2OS cells. We also detected a very weak signal with Tmod4 antibody, whereas Tmod2 was undetectable (Figure S1A). Immunofluorescence mi- croscopy demonstrated that endogenous Tmod1 and Tmod3 localize to stress fibers in U2OS cells (Figures 1A and S1B). Tmod3 displayed prominent localization to both contractile (ventral stress fibers and transverse arcs) as well as non-contractile (dorsal stress fibers) actin bundles, whereas endogenous Tmod1 was detected only in contractile actin bundles. Moreover, a small fraction of Tmod3 localized to the lamellipodia (Figures 1A and S1B). Please note that the observed nuclear localization with the Tmod3 antibody is likely an artifact resulting from unspecific antibody binding, because similar nuclear staining with this anti- body was also observed in Tmod3 knockout cells (Figure 1B).

To examine the functions of Tmod1 and Tmod3 in U2OS cells, we silenced Tmod1 by small interfering RNA (siRNA) (Figure 1C) and generated Tmod1 and Tmod3 knockout cell lines by CRISPR/Cas9 (Figures 1C, S1G, and S2A–S2D). Depletion of either isoform did not lead to drastic defects in the stress fiber networks of cells cultured on coverslips or on micro-patterned surfaces (Figures 1B and S1C–S1F). Interestingly, western blot analysis revealed elevated Tmod1 protein levels in the Tmod3 knockout cells compared to control cells (Figures 1C and 1D), as well as upregulation of Tmod3 in Tmod1 knockdown cells (Figures 1C and 1E). Tmod1 and Tmod3 also localized more prominently to stress fibers in the cells where the other isoform was absent (Figure 1B). Together, these data show that Tmod1 and Tmod3 are integral components of stress fibers and may have at least partially redundant roles in stress fiber assembly/ maintenance in osteosarcoma cells.

Depletion of Tmods Results in the Disappearance of Stress Fibers and in Consequent Defects in Force Generation

To address the functional roles of Tmods in stress fibers, we simultaneously depleted Tmod1 and Tmod3 from U2OS cells. This was achieved through acute depletion of Tmod1 by siRNA in the background of Tmod3 knockout cells (Tmod3 knockout [KO]+Tmod1 siRNA). Wild-type cells, as well as the cells where Tmod1 or Tmod3 were individually depleted, contained prominent stress fibers and mature focal adhesions, but the Tmod3 KO +Tmod1 siRNA cells (lacking both Tmod isoforms) dis- played almost complete loss of stress fibers and contained only very small focal adhesions (Figure 2A). Instead, these cells contained a dense, disorganized meshwork of actin filaments. A similar phenotype was observed in cells in which Tmod1 and Tmod3 were simultaneously depleted by siRNAs (Figures S2E–S2I). Quantification of the numbers of thick actin filament bundles revealed a small decrease in the amount of thick stress fibers in Tmod1 and Tmod3 knockout cells (Figure S1D). However, the numbers of thick actin bundles detected by this approach in Tmod3 KO+Tmod1 siRNA cells were severely reduced compared to control cells (Figure 2B). Additionally, the proportion of small focal adhesions was much higher in Tmod3 KO +Tmod1 siRNA cells compared to control cells and cells where the Tmod isoforms were depleted individually (Figures 2C and S1E). Because stress fibers are the major generators of contractile forces in many non-muscle cells [33], we examined the effects of Tmod depletion on cellular force generation. Tmod3 KO+Tmod1 siRNA cells displayed a significant reduction in traction-force generation compared to wild-type U2OS cells (Figures

2F and 2G). Together, these results show that Tmods are critical for maintenance of contractile stress fibers in U2OS cells. Consequently, their depletion results in severe defects in cell morphogenesis, force production, and the maturation of focal adhesions.

Tmods Stabilize Tropomyosin-Decorated Actin Filaments in Non-muscle Cells

In mammals, over 40 different tropomyosin isoforms can be generated from four *tropomyosin* genes through alternative splicing. Actin filaments in stress fibers are largely decorated by tropomyosins, which stabilize and functionalize these filaments [7]. Tmods display higher affinity to tropomyosin-decorated actin filament pointed ends compared to bare actin filaments [18, 19]. Therefore, we compared the localization of tropomyosins in wild- type versus Tmod3 KO+Tmod1 siRNA cells. Immunofluorescence microscopy using LC24 antibody, which detects tropomyosin isoforms Tpm2.1 and Tpm4.2, revealed that these tropomyosins faithfully localize to stress fibers in wild-type cells but display more diffuse localization in cells lacking Tmods (Figure 3A). Because earlier studies reported that many tropomyosin isoforms are unstable and degraded in the absence of actin filament templates [34, 35], we analyzed the protein levels of Tpm1.6/1.7/2.1 with TM311 and Tpm2.1/4.2 and Tpm3.1/3.2 with LC24 and Ɣ/9d antibodies, respectively. Western blot analysis revealed that depletion of Tmod3 alone resulted in only small decreases in Tpm1.6/1.7/4.2 protein levels, whereas the levels of Tpm2.1 and Tmp3.1/3.2 were not significantly affected. When Tmod1 was depleted, the levels of Tpm1.6/1.7/2.1 were unaltered, whereas the levels of Tpm2.1/4.2/3.1/3.2 were elevated compared to control cells. However, when both Tmod3 and Tmod1 were depleted, cells showed drastically lower levels of all the tropomyosin isoforms (Figures 3B and 3C).

Quantitative real-time PCR analysis revealed that the mRNA levels of Tpm1.7, Tpm3.1, and Tpm4.2 were not diminished by simultaneous depletion of Tmod1 and Tmod3, demonstrating that the decreases in the protein levels of these isoforms do not result from lower transcript levels. In contrast, the mRNA levels of Tpm1.6, which is generated through alternative splicing from the same gene as Tpm1.7, were drastically reduced in the Tmod3 KO+Tmod1 siRNA cells (Figure S3B). However, the Tpm1.6 mRNA levels were similarly diminished in Tmod1 siRNA cells and Tmod3 KO cells (Figure S3C), which do not display a strong stress fiber phenotype (Figures 1B and S3A). Thus, although the depletion of Tmod1 and Tmod3 (either individually or together) affects the alternative splicing of *TPM1* gene, the resulting decrease in the Tpm1.6 mRNA level does not affect the organization of stress fibers.

In addition to the loss of stress fibers, the Tmod-depleted cells typically contained more pronounced lamellipodia-like protrusions, as detected by an antibody against the Arp2/3 complex, compared to the wild-type U2OS cells (Figures 2D and 2E). To further test whether the loss of Tpm-decorated actin filaments and an increase of lamellipodial width result from Tmod depletion, we performed rescue experiments using GFP-tagged Tmod3 (GFP-Tmod3). The cells were stained with phalloidin to visualize F-actin, with LC24 antibody to visualize Tpm2.1/Tpm4.2, and with cortactin and Arp2/3 antibodies to visualize Arp2/3-rich lamellipodia-like protrusions. Expression of GFP-Tmod3 in the Tmod3 KO +Tmod1 siRNA cells led to a re-appear- ance of stress fibers that also contained

tropomyosins (Figure 4A). Moreover, the total tropomyosin intensities were higher in rescue cells compared to the Tmod- depleted cells that did not express GFP- Tmod3 (Figure 4B). Finally, the increased lamellipodial width in Tmod-depleted cells was rescued by expressing GFP-Tmod3 (Figures 4A and 4C).

We also examined the roles of Tmod1 and Tmod3 in human dermal fibroblasts (HDFs). Simultaneous depletion of Tmod1 and Tmod3 by siRNA in these cells resulted in a depletion of tropomyosin isoforms and a concomitant reduction of stress fibers, similar to what was observed in U2OS cells (Figures S3D–S3F). However, we did not observe robust lamellipodia formation in Tmod1/Tmod3 siRNA cells compared to wild-type HDF cells. This is most likely due to lack of lamellipodia in HDF cells, at least when plated on fibronectin. Together, these results provide evidence that Tmods are critical for maintaining the stability of tropomyosin-decorated actin filaments in non-muscle cells. In the absence of Tmods, most tropomyosins do not associate with actin filaments and are destined for degradation.

Tmods Stabilize Tropomyosin-Decorated Actin Filaments in Non-muscle Cells

In addition to an actin-binding site (ABS1), the N-terminal region of Tmods harbors two tropomyosin-binding sites (TMBS1 and TMBS2) [19]. The TMBSs are important for capping Tpm-deco- rated actin filaments with high-affinity *in vitro* [18, 20]. However, the functional importance of the two TMBSs and Tmod-Tpm interactions in the context of actin dynamics has not been addressed. We mutated the TMBS1 and TMBS2 domains of Tmod3. The mutant was generated by replacing highly conserved leucine residues with aspartic acid at four locations in TMBS1 (L29D, L32D, L36D, and L39D) and TMBS2 (L131D, L134D, L138D, and L143D), which should disrupt interactions with the Tpm coiled-coil (Figure 5A). Using the pyrene-actin fluorescence assay, we determined the maximum elongation rate of actin in the presence of wild-type and mutant Tmod3, both with and without Tpm. Representative experiments illustrate the fluorescence increase upon incorporation of actin monomers into Tmod3-capped actin filaments at various concentrations of Tmod3 (Figures S4A and S4C). Saturating CapZ (25 nM) was added to block monomer incorporation into the barbed end of the filaments [18]. Instantaneous slopes were calculated to determine the time intervals corresponding to the maximum elongation rate at each Tmod3 concentration (Figures S4B and S4D) and normalized to the control maximum elongation rate in the absence of Tmod. In the absence of Tpm, wild-type and mutant Tmod3 showed equal capping activities (Figure 5B), whereas in the presence of Tpm, the mutant had significantly reduced capping activity (Figures 5C, S4E, and S4F). These re- sults suggest that the TMBSs of Tmod3 are critical for the bind- ing of Tpm and efficient filament pointed end capping *in vitro*.

Given the reduced capping activity of Tmod3-TMBS mutant in the *in vitro* assays, we performed rescue experiments by ex- pressing wild-type GFP-Tmod3 and the GFP-Tmod3 TMBS mutant in Tmod3 KO+Tmod1 siRNA cells. Wild-type GFP-Tmod3 was either detected in stress fibers or displayed rather diffuse localization, depending on the expression level. Importantly, wild-type GFP-Tmod3 was able to rescue the dis- rupted stress fibers in Tmod-depleted cells, but the Tmod3 TMBS mutant displayed mainly diffuse cytoplasmic or

nuclear localization and failed to rescue the stress fibers phenotype (Figures 5D, 5E, S5A, and S5B). Moreover, wild-type Tmod3 rescued the focal adhesion size distribution defect close to the control cell level, but the Tmod3 TMBS mutant expression could not rescue this phenotype (Figure S5C). Finally, expression of wild- type GFP-Tmod3 partially rescued the loss of tropomyosins in Tmod3 KO+Tmod1 siRNA cells, whereas the Tmod3 TMBS mutant was much less efficient in rescuing the diminished levels of tropomyosins in these cells (Figures 5F and S5D). Together, these data uncover a functional role of TMBSs of Tmod in its ability to promote efficient pointed end capping of tropomyosin-decorated actin filaments *in vitro* and in stabilization of tropomyosin-decorated actin filament structures in cells.

Tmods Maintain the Balance between Tropomyosin- Actin Filaments and Arp2/3-Complex-Assembled Actin Filament Structures

In unicellular yeasts, tropomyosin-decorated actin filaments are nucleated and polymerized by formins [36, 37], whereas protrusive branched actin networks do not contain detectable levels of tropomyosins and are mainly nucleated by the Arp2/3 complex [6]. Therefore, we examined the possible connections between Tmod-stabilized tropomyosin-actin filaments and the Arp2/3 complex. We first inhibited Arp2/3 complex by incubating wild-type U2OS cells in the presence of 100 mM CK666, a well- established Arp2/3 complex inhibitor [38]. The tropomyosin levels were not drastically altered, and stress fibers were still pre- sent in CK666-treated cells. However, instead of a combination of ventral stress fibers, transverse arcs, and dorsal stress fibers, the Arp2/3-complex-inhibited cells contained predominantly ventral stress fibers that were anchored to large focal adhesions at both the ends (Figures S6B–S6F). The efficiency of CK666 treatment was confirmed with an antibody against P34, which demonstrated that Arp2/3 complex localized to lamellipodial edges in wild-type U2OS cells but was largely absent from lamellipodia of CK666-treated cells (Figure S6B).

Importantly, treatment of Tmod1/3-depleted cells with the Arp2/3 complex inhibitor led to a partial rescue of the phenotype. This is because CK666-treated Tmod3 KO+Tmod1 siRNA cells harbored more stress fibers compared to the untreated cells (Figure 6A). They also displayed larger focal adhesions and were less circular (Figures 6B and 6C). Moreover, treatment of Tmod3 KO+Tmod1 siRNA cells with CK666 led to elevated tropomyosin protein levels, and we could also detect some tropomyosin localization to stress fibers in these cells (Figures 6E and S6A). Similar rescue of the stress fiber phenotype and tropomyosin levels was also observed when the ARPC2 subunit of the Arp2/3 complex was depleted by siRNA in the Tmod3 KO+Tmod1 siRNA cells (Figures 6A, 6D, and 6E).

Taken together, these data provide evidence that Tmods stabilize tropomyosin-actin filaments in non-muscle cells. Depletion of Tmods leads to an unbalance between tropomyosin-actin filaments and Arp2/3-nucleated branched actin filament structures, and this can be partially rescued by inhibition of the Arp2/3 complex.

DISCUSSION

The function of Tmods has been best characterized in the context of muscle myofibrils, where they prevent actin filaments from overgrowth. Here, we show that, in non-muscle cells (U2OS osteosarcoma cell line and human dermal fibroblasts), Tmods do not prevent

actin filaments from excessive growth but are instead critical for stabilizing tropomyosin-decorated actin filaments. In the absence of Tmods, the tropomyosin-decorated actin filaments disassemble. This also leads to degradation of tropomyosins, because most tropomyosins are unstable in the absence of an actin filament template [35]. At least in budding yeast, tropomyosin-decorated actin filaments are nucleated and elongated by formins [36, 37]. Thus, we propose that depletion of Tmods results in a shift in the balance between formin- and Arp2/3-complex-nucleated actin filament networks and leads to a consequent loss of stress fibers and in an excess of Arp2/3-complex-nucleated, branched actin filament networks (Figure 7). Previous studies demonstrated that the Arp2/3-complex-nucleated and formin- and Ena/VASP-polymerized actin filament structures compete with each other for a limited pool of assembly-competent actin monomers in cells. Small actin monomer-binding protein, profilin, controls the homeostasis be- tween these networks by preferentially delivering actin monomers to Ena/VASP and formins [11, 12]. Our results show that not only regulation of actin filament assembly but also regulation of actin filament disassembly by Tmods is critical for maintenance of the homeostasis between these actin filament networks in cells. Our data also suggest that tropomyosin-decorated actin filaments have a higher need for filament pointed end stabilization compared to the branched Arp2/3 complex-nucleated net- works. This may be because, within the branched actin filament networks, majority of filament pointed ends are capped by the Arp2/3 complex, at least until the filaments become severed by ADF/cofilins [39]. This may provide an explanation for the importance of Tmods in stabilizing tropomyosin-decorated, linear actin filaments in non-muscle cells. Moreover, the lamellipodial actin filament networks are more dynamic compared to stress fibers [5, 15]. Thus, actin filament assembly is probably slower in stress fibers compared to Arp2/3-nucleated networks, and thus, also filament disassembly must be slower in stress fibers to maintain the balance between these actin filament arrays.

Our data suggest that Tmods have different effects on actin dynamics in myofibrils of muscle versus stress fibers of non- muscle cells. Previous studies demonstrated that Tmods are negative regulators of thin filament length in muscle cells [13, 25, 26], although our work demonstrates that loss of Tmods leads to disassembly of functionally similar actin filaments in contractile stress fibers. In this context, it is important to note that actin filament assembly appears to display differences in muscle versus non-muscle cells. This is because actin filaments in muscle sarcomeres can elongate through actin filament assembly at both filament barbed and pointed ends [13], whereas actin filament elongation in non-muscle cells occurs predominantly through filament polymerization at barbed ends. We speculate that the sizes of actin monomer pools may differ between muscle and non-muscle cells. A large pool of assembly-competent actin monomers in muscle cells would allow filament elongation at both barbed and pointed ends, and thus, depletion of Tmods results in overgrowth of tropomyosin-decorated actin fil- aments. On the other hand, non-muscle cells may have a limited pool of assembly-competent actin monomers [11], and thus, depletion of Tmods does not accelerate elongation of tropomyosin-decorated actin filaments at their pointed ends but instead leads to their depolymerization. Alternatively, the differences in the roles of Tmods in muscle versus non-muscle cells may result from different actin and tropomyosin isoforms expressed in these cells. In a wider context, these data imply that the

same biochemical activity of an actin-binding protein can have opposite effects in cells depending on the cell type.

Our work provides mechanistic insights into the function of Tmods in non-muscle cells. Previous studies linked Tmods to cell migration, insulin-stimulated exocytosis, and formation of adherens junctions in epithelial cells [28, 30, 31]. Moreover, actin filament and tropomyosin (Tpm4.2) organizations are abnormal in *Tmod3*$^{-/-}$ embryo megakaryocytes during platelet biogenesis [23], and mouse lenses lacking Tmod1 were reported to have diminished levels of g (Tpm3)-tropomyosin [40, 41]. However, the precise mechanism by which Tmods contribute to these processes has remained elusive. We propose that Tmods control these processes though stabilization of tropomyosin-decorated actin filaments and by maintaining the homeostasis between the Arp2/3 complex- and formin-nucleated actin filament networks. For example, Tmod3 was shown to be a negative regulator of actin filament assembly at lamellipodia [31]. This can be explained by our work demonstrating that inhibition of Tmods increases the amounts of Arp2/3-complex-nucleated actin filaments in cells. Because, in addition to stress fibers, Tmod3 also localizes to lamellipodia, it is possible that Tmod3 addition- ally stabilizes specific tropomyosin-decorated actin filaments within the lamellipodium. Indeed, previous studies reported that, in addition to the Arp2/3-complex-nucleated actin filament networks, lamellipodia also contain actin filaments decorated by tropomyosins [42]. Also, adherens junctions are composed of both Arp2/3-complex-nucleated actin filament structures as well as tropomyosin-containing contractile actin filament arrays [43, 44]. Thus, depletion of Tmod3 may shift the balance be- tween different actin filament structures, like shown here for U2OS cells, and result in consequent problems in epithelial morphogenesis. Finally, insulin-stimulated exocytosis was shown to involve at least one tropomyosin isoform (Tpm3.1) [28, 45]. Thus, it is possible that, also in this process, Tmod3 stabilizes Tpm3.1-decorated actin filaments that are necessary for exocytosis.

Collectively, our work reveals that Tmods specifically cap tropomyosin-decorated actin filaments in cells. Depending on the cell type, and probably on the size of assembly-competent actin monomer pool, Tmods either stabilize tropomyosin-deco- rated actin filaments or prevent them from excessive polymerization. Through their ability to stabilize tropomyosin-decorated actin filaments, Tmods are critical for maintaining the homeostasis between protrusive (Arp2/3-complex-nucleated) and contractile (formin-nucleated) actin filament networks at least in non-muscle cells. An important remaining question concerns the need of several different Tmod isoforms in mammals. Our work demonstrates that Tmod1 and Tmod3 have redundant functions in stabilizing the tropomyosin-decorated actin filament structures in osteosarcoma cells. However, Tmod1 and Tmod3 display minor differences in their subcellular localizations, and their individual depletions resulted in slightly different phenotypes, e.g., concern- ing the protein levels of tropomyosin isoforms. It is possible that different Tmod isoforms exhibit some specificity toward certain tropomyosin isoforms and may thus stabilize partially non-over- lapping populations of tropomyosin-decorated actin filaments in cells. Moreover, Tmod isoforms display biochemical differences. This is because, in addition to actin filament pointed end capping, Tmod3 can bind and sequester actin monomers at least *in vitro* [21]. The possible *in vivo* importance of this activity of Tmod3 should be examined in the future. Finally, Tmods have

been associated with various diseases. Elevated levels of Tmod1 and Tmod3 were linked to progression of oral and liver cancers, respectively [46, 47]. Tmod3 was also associated to chemoresistance of non-small cell lung cancer [48]. In the future, it will be important to uncover the precise mechanisms by which Tmods contribute to these human disorders.

EXPERIMENTAL MODEL AND SUBJECT DETAILS

Cell culture and transfection

Human osteosarcoma (U2OS) cells (derived from a fifteen-year-old human female suffering from osteosarcoma) and Human dermal fibroblast (HDF) cells (derived from the dermis of normal male neonatal foreskin) were maintained in high-glucose (4.5 g/l) Dulbecco's modified Eagle's medium (DMEM) [BE12–614F; Lonza], supplemented with 10% Fetal Bovine Serum [10500–064; GIBCO], 10 U/ml penicillin, 10 mg/ml streptomycin, and 20 mM L-glutamine [10378–016; GIBCO] referred to as complete media at 37C in humidified atmosphere with 5% CO_2. Transient transfections were performed with Fugene HD (Promega) according to manufacturer's instructions using 3.5:1 Fugene/DNA ratio, and cells were incubated for 24 h before fixation with 4% paraformaldehyde (PFA) in phosphate-buffered saline (PBS). However, a 48 h incubation before fixation was used for rescue experiments. siRNA knockdowns were performed with INTEFERin (PolyPlus Transfection) according to manufacturer's instructions, using 40 nM of On-target plus human Tmod1 SMART pool siRNA (TMOD1 Target sequences: 5^0 CCUCAAUAAUAUCCGGAAU 3^0, 5^0 GGAAACGCUGGAACGGAUA 3^0, 5^0 GUAAUGACCCCGUGGCGUA 3^0, 5^0 ACGCAAUGAUGAACAACAA 3^0), On-target plus human Tmod3 SMART pool siRNA (TMOD3 Target sequences: 5^0 CAGCAGGGACCACGAACCA 3^0, 5^0 ACAAUGACUUAGUGCGUAA 3^0, 5^0 GCGUUAAGAGAUAAU GAAA 3^0, 5^0 GUAUAGUGAGGUCGAAGUU 3^0), On-target plus human ARPC2 siRNA (ARPC2 Target sequences: 5^0 CCAUGUAUG UUGAGUCUAA 3^0, 5^0GCUCUAAGGCCUAUAUUCA 3^0, 5^0 GGACAGAGUCACAGUAGUC 3^0, 5; GUACGGGAGUUUCUUGGUA 3^0. 40 nM AllStars siRNA (QIAGEN) was used as negative-control in all siRNA experiments, and it did not result in detectable pheno-type in any of the assays performed. 72–96 h incubation period was used to efficiently deplete the target proteins. In the case of rescue experiments, siRNA transfection was repeated after 72 h to make sure that the target protein remained depleted. Arp2/3 complex – inhibition was done with 100 mM CK666 (Sigma) dissolved in DMSO (10 mM stock) and added directly to complete media (DMEM with 10% FBS) with incubation times of 7–8 h at 37C.

METHOD DETAILS

BioID screening

BioID analysis for tropomyosin 3.1 was performed as described in [49–51]. To obtain a plasmid for expressing BirA fused to the N terminus of Tpm3.1, human Tpm3.1 cDNA was amplified and subcloned into the pcDNA3.1 mycBioID vector (Addgene). For proteomics, cells growing on five 14.5 cm tissue culture plates were transfected with the plasmid using FuGENE HD transfection reagent (Promega) according to the manufacturer's instructions. Backbone vector pmycBioID-C1 was transfected as control. Cells were grown for 24 h

without biotin and another 24 h in the presence of 50 mM biotin. Single-step affinity purifications of the biotinylated proteins, as well as liquid chromatography mass spectrometry sample preparation, and mass spectrometry were performed as in [50]. To obtain a list of high-confidence protein interactions for Tpm3.1 the data were filtered against our in-house BioID contaminant database.

CRISPR knockout generation

Tmod3 and Tmod1 CRISPR knock-out cell lines were generated as described previously [2, 49]. Guide sequence targeting exon 1 of the human *TMOD3* gene and exon 5 of *TMOD1* gene were selected based on the CRISPR Design Tool, with a quality score of 91 and 93 respectively. Oligonucleotides for cloning guide RNA into pSpCas9 (BB)-2A-GFP vector (48138; a gift from F. Zhang, Addgene, Cambridge, MA) were designed as described previously [52]. Transfected cells were sorted with FACSAria II (BD), using low intensity GFP-positive pass gating, as single cells onto a 96-well plate, supplemented with DMEM containing 20% FBS and 10 mM HEPES buffer. For this study, two CRISPR clones (T3–2 and T3–5) were selected based on lack of detectable Tmod3 protein by western blot.

The observed phenotypes (loss of stress fibers and depletion of tropomyosins when combined with Tmod1 siRNA) of both clones were very similar to each other. The data presented in the manuscript are from the T3–2 clone. In order to further confirm the CRISPR Tmod3 knockout, the genomic region surrounding the target sequence region was amplified using primers 5^0 AGAGACCGCACAGG AAGGAAATG 3^0 and 5^0 GAGACAGAGGTTGGCGTGTATC 3^0, for Sanger sequencing analysis. Moreover, Illumina Next Generation Sequencing (NGS) was performed using primers 5^0 ACACTCTTTCCCTACACGACGCTCTTCCGATCTATTAAGTGACTTGCTGC CCTG 3^0 and 5^0 GTGACTGGAGTTCAGACGTGTGCTCTTCCGATCTTTGGATAAAGTGGAGGAAAGG GTG 3^0. Consistent with the Sanger sequencing data, NGS analysis of 3085743 reads revealed that 99.7% of the obtained sequences harbored a single nucleotide insertion that results in a translational frameshift, and no wild-type alleles were detected. For Tmod1, the CRISPR knockout clone was selected based on undetectable Tmod1 protein level in western blot. Similar to Tmod3 CRISPR validation, we performed Sanger sequencing and NGS on amplified surrounding region of target sequence of TMOD1 by using primers 5^0 CTGGGATGGTCAA ATGGGCT 3^0, 5^0 AGGCAGGGCTAGTCATTTTCC 3^0 and 5^0 ACACTCTTTCCCTACACGACGCTCTTCCGATCTTTCTTGCCATTT CTGTGAGCC 3^0, 5^0 GTGACTGGAGTTCAGACGTGTGCTCTTCCGATCTTCAGTGAGTGGAGGAAGCAAG 3^0 respectively. NGS anal- ysis of 541146 reads demonstrated lack of wild-type Tmod1 sequence, and three different major modifications: insertion of five nucleotides, deletion of two nucleotides, and insertion of two nucleotides with frequencies of 89.9%, 4.8%, and 3.9%, respectively. This indicates that the Tmod1 knockout cells indeed display complete loss of Tmod1, but they appear to consist of a combination of at least two cell-clones where the Tmod1 alleles were disrupted differently. Alternatively, the observed different modifications may result from aneuploidy (i.e., the three modified alleles could derive from a single clone with multiple alleles).

Plasmids

Human Tmod3 cDNA (pANT7_cGST) was purchased from DNASU Plasmid Repository (HsCD00629766). Plasmids for expressing wild-type human GFP-Tmod3 and GFP-Tmod3 TMBS mutant were cloned into pEGFPC1 vector using NEBuilder kit (NEB, #E5520S), and the point mutations in Tmod3 TMBS were introduced by PCR in the Tmod3 cDNA. Tmod3 wild-type and TMBS mutant were cloned between the NdeI and SapI sites of vector pTXB1 (New England BioLabs) containing a chitin affinity tag and an intein domain for purification. Plasmids used in this study are also listed in the Table S2.

Western Blotting

All cell lysates were prepared by washing the cells once with PBS and scraping them into lysis buffer (50 mM Tris-HCl pH 7.5 150 mM NaCl, 1 mM EDTA, 10% Glycerol, 1% Triton X-100) supplemented with 1 mM PMSF, 10 mM DTT, 40 mg/ml DNase I and 1 mg/ml of leupeptin, pepstatin, and aprotinin. All preparations were conducted at 4C. Protein concentrations were determined with Bradford reagent (#500–0006, Bio-Rad) and equal amounts of the total cell lysates were mixed with Laemmli Sample Buffer, boiled, and run on 4%–20% gradient SDS-PAGE gels (#4561096, Bio-Rad). Proteins were transferred to nitrocellulose membrane with Trans-Blot Turbo transfer system (Bio-Rad) using Mini TGX gel transfer protocol. Membrane was blocked in either 5% milk-TBS with 0.1% Tween20 (TBST) or with 5% BSA for one hour at RT. Primary and secondary antibodies were diluted into fresh blocking buffer for overnight at 4C and one hour at room temperature, respectively. Proteins were detected from the membranes with Western Lightning ECL Pro substrate (PerkinElmer). Band-intensity quantification from the western blots was performed with ImageJ densitometry analysis [53], and normalized to GAPDH protein levels.

Immunofluorescence Microscopy

Immunofluorescence (IF) experiments were performed as previously described [2, 49]. Briefly, cells were fixed with 4% PFA in PBS for 15 min at RT, washed three times with 0.2% BSA in Dulbecco's phosphate buffered saline, and permeabilized with 0.1% Triton X-100 in PBS for 5 min. Cells were blocked in 1 3 Dulbecco PBS supplemented with 0.2% BSA. Both primary and secondary anti- bodies were applied onto cells and incubated at RT for 1 hour. Alexa-conjugated phalloidin was added together with primary anti- body solutions onto cells. All IF data were obtained with a Leica DM6000B wide-field fluorescence microscope with a HCXPL APO 63 3 1.40–0.60 NA oil objective, except for IF images used for lamellipodia width analysis that were obtained with upright Leica SP8 confocal microscope with HC PL APO 63x/1.30 GLYC CORR CS2 objective. For micro-pattern experiments, the cells were plated on CYTOOchipsTM prior to fixation as described previously [49]. The following antibodies were used for the study. Mouse mono- clonal Tropomodulin 1 (TMOD1) antibody (NBP2–00955) was from Novusbio (working dilutions, 1:100 for IF and 1:200 for WB). Rabbit polyclonal Tropomodulin 2 (TMOD2) antibody (HPA041365) was from Sigma (working dilution, 1:100 for WB). Rabbit polyclonal Tropomodulin 3 (TMOD3) antibody (NBP1–86870) was from Novusbio (working dilutions, 1:50 for IF and 1:100 for WB). Rabbit polyclonal Tropomodulin 4 (TMOD4) antibody (SAB1101538) was from Sigma (working dilution, 1:100 for WB). Mouse monoclonal

TM311 anti- body (T-2780) was from Sigma (working dilutions, 1:200 for IF and 1: 1000 for WB). Mouse monoclonal LC24 antibody (working dilutions, 1:200 for IF and 1:500 for WB). Mouse monoclonal Gamma 9d antibody (working dilution 1:200 for WB). The generation, specificity and conditions of use of all the tropomyosin antibodies are as previously published [54]. Rabbit polyclonal Vinculin anti- body (ab73412; 1:200 for IF) and rabbit polyclonal GAPDH antibody ((ab29330; 1:1000 for WB) were purchased from Abcam. Mouse monoclonal Vinculin antibody (V9131) was purchased from Sigma (working dilution, 1:400 for IF). Rabbit polyclonal P34 antibody (07–227) was purchased from EMD Millipore (working dilution, 1:200 for IF). Mouse monoclonal Cortactin antibody (05–180) was from EMD Millipore (working dilution, 1:200 for IF). F-actin was visualized with Alexa Fluor 488, 568 and 647 conjugated to phalloidin (1:200 IF). The following secondary antibodies were used for the study. Alexa Fluor goat anti–mouse 488 (A11001), 568 (A11004), and 647 (A31571); Alexa Fluor goat anti–rabbit 488 (A11034), 568 (A11010) and 647 (A21245; all 1:200–1,000 IF); and both HRP-conjugated goat anti–rabbit (G-21234) and HRP-conjugated goat anti–mouse (G-21040; both 1:5,000 WB) antibodies, were from ThermoFisher Scientific.

Traction Force Microscopy

For traction force imaging experiments, fibronectin-1-coated elastic polyacrylamide (PAA) gels with known stiffness (elastic modulus = 26 kPa) were prepared. Sulfo-SANPAH (Sigma-Aldrich) was used as a linker in between the substrate and fibronectin-1. Before coating with fibronectin-1, substrates were covered with sulfate fluorescent microspheres (Invitrogen, diameter 200 nm; excitation wavelength 488) for monitoring bead displacement. U2OS cells were cultured on these PAA-gels and plating was done at least 2 h prior to imaging. Cells and the underlying microspheres were imaged with 3I Marianas imaging system containing a heated sam- ple chamber (+37C) and CO_2 control (3I intelligent Imaging Innovations, Germany). 63x/1.2 W C-Apochromat Corr WD = 0.28 M27 objective was used. After the first set of images, cells were detached from the substrates with 10 x Trypsin (Lonza) and a second set of microsphere images were taken to serve as reference images. Displacement maps were achieved by comparing the reference micro- sphere images to the first set of images and by calculating the displacement field and substrate stiffness, cell-exerted traction fields were computed by using Fourier Transform Traction Cytometry [55, 56]. Analyses was performed blind and cell borders were manually traced. Root mean squared magnitudes were computed from the traction fields.

Filament analysis (Ridge detection)

The total number of stress fibers, as well as the number of thick actin filament bundles in U2OS cells were quantified with Ridge detection plugin from Fiji ImageJ. The parameters used for quantifying the total number of stress fibers were: line width 20.0, high contrast 230, low contrast 100, sigma 6.57, low threshold 0.0, and upper threshold 0.34. The parameters used for quantifying the thick bundles were: line width 29.0, high contrast 230, low contrast 87, sigma 8.87, low threshold 0.0, and upper threshold 0.17. Please note that approximately 20%–30% of Tmod1 siRNA transfected Tmod3 KO cells still showed relatively strong cytoplasmic staining of Tmod1 by immunofluorescence microscopy, and these were excluded from all immunofluorescence-based analyses.

Focal adhesion quantification

Focal adhesion areas in U2OS cells were manually quantified with ImageJ, measuring the size of each individual adhesion with the ROI manager and freehand tool in Fiji ImageJ. Cells that adhered to several neighbors were discarded from the analysis. From trans- fected cells, only those displaying low or moderate GFP intensity were selected for analysis. Adhesions were classified into seven size groups, and the percentage ratio of the focal adhesions in each class was obtained by dividing the focal adhesion number of individual size classes with the total number of focal adhesions in the same cell.

Tropomyosin intensity quantification

Normalized relative total fluorescence intensities of Tpm 2.1/4.2 (detected by LC24 antibody) were quantified from immunofluorescence images of wild-type and non-transfected and GFP-Tmod3 expressing Tmod3 knockout + Tmod1 siRNA cells from the same image. The corrected total cell fluorescence (CTCF) was calculated using the formula: CTCF = Integrated Density – (Area of selected cell * mean fluorescence of background readings) in Fiji ImageJ.

Lamellipodia quantification

Width of lamellipodia in wild-type, Tmod3 KO + Tmod1 siRNA and Tmod3 siRNA^{+} Tmod1 siRNA U2OS cells were manually quantified from p34 (against Arp2/3 complex) - stained cells by using constant line segmentation with ROI manager and intensity plot profile tools from the position of thickest Arp2/3-rich lamellipodium/protrusion with Fiji ImageJ. Likewise, widths of lamellipodia in rescue experiments were similarly quantified and compared to wild-type, untransfected and GFP-Tmod3 transfected Tmod3 knock-out + Tmod1 siRNA U2OS cells. From transfected cells, only those displaying low or moderate GFP intensity were selected for analysis.

Real-time quantitative PCR

Total mRNAs were extracted with the GeneJET RNA purification kit (K0731; Thermo Fisher Scientific) and single-stranded cDNA was synthesized (K1671; Thermo Fisher Scientific) from 500 ng of the extracted mRNA. Primers amplifying region for Tpm1.6, Tpm 1.7 Tpm 3.2, Tpm 4.2 and *GAPDH* were designed with the Primer-BLAST tool [57]. Quantitative PCR reactions were performed with Maxima SYBR Green/ROX (K0221; Thermo Fisher Scientific) in LightCycler 480 Instrument II (Roche). Changes in expression levels were calculated with the $2^{"DDCt}$ method, and normalized to GAPDH (DCt) and WT expression levels, respectively.

Protein purification

Wild-type and TMBS mutant Tmod3 in pTXB1 were expressed in *E. coli* BL21 (DE3) cells (Invitrogen) grown in Terrific Broth medium at 37C until the OD600 reached a value of 1–1.5. Expression was induced with 0.3 mM IPTG, and was carried out for 16 h at 19C. Cells were harvested by centrifugation, re-suspended in chitin buffer (HEPES-20mM-pH 7.5, NaCl-500mM, EDTA-1mM, DTT-1mM, PMSF-1mM), and lysed using a microfluidizer apparatus (Microfluidics). Proteins were first purified on a chitin affinity column, and eluted

after selfcleavage of the intein induced by incubation with 40 mM DTT for 24 h. Proteins were then purified through a SD200HL 26/600 gel filtration column (GE Healthcare) in HEPES-20mM-pH 7.5, NaCl-200mM, EDTA-1mM, DTT-1mM. Fractions containing Tmod were dialyzed overnight to HEPES-20mM, NaCl-50mM, loaded on an ion exchange sourceQ column (Pharmacia), and eluted with a 50–500 mM NaCl gradient. CapZ protein was purified as described [18]. Briefly, both subunits (alpha and beta) were cloned into both cloning sites of pRSFDuet-1 vector (Novagen) which includes a 6x-His tag and a TEV cleavage site [18]. Purification was carried out as described previously [18]. Actin [58] and tropomyosin [59] were purified as described.

Pointed-end capping assay

Capping assays were carried out as described previously [18]. Briefly, 1.5 mM G-actin (6% pyrene-labeled), 1.5 mM filament seeds, 25 nM CapZ, +/” 1 mM Tpm were used. Tmod3 was used at 6 different concentrations (25, 50, 100, 200, 400, 800 nM). Pyrene fluorescence (excitation 365 nm, emission 407 nm) was detected using a plate reader (BioTekCytation 5). For each Tmod3 concentration, four replicates were recorded. Maximum polymerization rates were determined by taking the first derivative of each curve, identifying the time interval corresponding to the greatest slope, and performing a linear regression on the original data within that time interval. For each concentration, the statistical analysis of the difference between the mean maximum polymerization rate was calculated using Bayesian statistics, by finding the posterior probability distribution for the difference in means (Tmod3 mutant relative to WT).

QUANTIFICATION AND STATISTICAL ANALYSIS

Statistical data analyses were performed with Excel (Microsoft) and Origin (Origin 2018b). Normality of the data was examined with the Shapiro-Wilk test and a quantile–quantile plot. For the data following normal distribution, Student’s two-sample unpaired t test was used. If data did not follow normal distribution, Mann-Whitney u-test for two independent samples was conducted. For RMS traction analysis no raw images were excluded with the exception of cells that were not in focus or the ones with the cell boundaries beyond the frame size. For filament analysis by Ridge detection in Fiji ImageJ, the obtained results for individual filaments was cross- checked with the original 8-bit raw images to avoid any default software miscalculations. Geneious (Biomatters Limited) analysis tool was used for constructing sequence alignments for Tmod3KO confirmation (Figures S2A and S2B).

DATA AND CODE AVAILABILITY

This study did not generate any unique code. The authors declare that all data supporting the findings of this study are available within the manuscript and its supplementary files or are available from the corresponding author on request.

Supplementary Material

Refer to Web version on PubMed Central for supplementary material.

ACKNOWLEDGMENTS

The authors thank Velia Fowler for discussions. This study was supported by grants from Sigrid Juselius Foundation, Jane and Aatos Erkko Foundation, and Cancer Society Finland (to P.L.). Y.J. was supported by “100 talents program” from the Chinese Academy of Sciences, Shanghai Talents Development Funding, National Natural Science Foundation of China (31970660), and Natural Science Foundation of Shanghai (19ZR1463000). R.K. was supported by a PhD student fellowship from Doctoral School in Health Sciences. P.W.G. received grants from the Australian National Health and Medical Research. P.J.C. and R.D. were supported by NIH grants T32 AR053461 and R01 GM073791, respectively.

REFERENCES

1. Blanchoin L, Boujemaa-Paterski R, Sykes C, and Plastino J (2014). Actin dynamics, architecture, and mechanics in cell motility. Physiol. Rev 94, 235–263. [PubMed: 24382887]
2. Lehtima€ki JI, Fenix AM, Kotila TM, Balistreri G, Paavolainen L, Varjosalo M, Burnette DT, and Lappalainen P (2017). UNC-45a pro- motes myosin folding and stress fiber assembly. J. Cell Biol 216, 4053– 4072. [PubMed: 29055011]
3. Campellone KG, and Welch MD (2010). A nucleator arms race: cellular control of actin assembly. Nat. Rev. Mol. Cell Biol 11, 237–251. [PubMed: 20237478]
4. Skau CT, and Waterman CM (2015). Specification of architecture and function of actin structures by actin nucleation factors. Annu. Rev. Biophys 44, 285–310. [PubMed: 26098516]
5. Lai FPL, Szczodrak M, Block J, Faix J, Breitsprecher D, Mannherz HG, Stradal TE, Dunn GA, Small JV, and Rottner K (2008). Arp2/3 complex interactions and actin network turnover in lamellipodia. EMBO J. 27, 982–992. [PubMed: 18309290]
6. Michelot A, and Drubin DG (2011). Building distinct actin filament net- works in a common cytoplasm. Curr. Biol 21, R560–R569. [PubMed: 21783039]
7. Gunning PW, Hardeman EC, Lappalainen P, and Mulvihill DP (2015). Tropomyosin - master regulator of actin filament function in the cytoskeleton. J. Cell Sci 128, 2965–2974. [PubMed: 26240174]
8. Gateva G, Kremneva E, Reindl T, Kotila T, Kogan K, Gressin L, Gunning PW, Manstein DJ, Michelot A, and Lappalainen P (2017). Tropomyosin isoforms specify functionally distinct actin filament popula- tions in vitro. Curr. Biol 27, 705–713. [PubMed: 28216317]
9. Burke TA, Christensen JR, Barone E, Suarez C, Sirotkin V, and Kovar DR (2014). Homeostatic actin cytoskeleton networks are regu- lated by assembly factor competition for monomers. Curr. Biol 24, 579–585. [PubMed: 24560576]
10. Suarez C, and Kovar DR (2016). Internetwork competition for mono- mers governs actin cytoskeleton organization. Nat. Rev. Mol. Cell Biol 17, 799–810. [PubMed: 27625321]
11. Rotty JD, Wu C, Haynes EM, Suarez C, Winkelman JD, Johnson HE, Haugh JM, Kovar DR, and Bear JE (2015). Profilin-1 serves as a gatekeeper for actin assembly by Arp2/3-dependent and -independent pathways. Dev. Cell 32, 54–67. [PubMed: 25543281]
12. Suarez C, Carroll RT, Burke TA, Christensen JR, Bestul AJ, Sees JA, James ML, Sirotkin V, and Kovar DR (2015). Profilin regulates F-actin network homeostasis by favoring formin over Arp2/3 complex. Dev. Cell 32, 43–53. [PubMed: 25543282]
13. Littlefield R, Almenar-Queralt A, and Fowler VM (2001). Actin dy- namics at pointed ends regulates thin filament length in striated muscle. Nat. Cell Biol 3, 544–551. [PubMed: 11389438]
14. Skwarek-Maruszewska A, Hotulainen P, Mattila PK, and Lappalainen P (2009). Contractility-dependent actin dynamics in cardiomyocyte sar- comeres. J. Cell Sci 122, 2119–2126. [PubMed: 19470580]
15. Hotulainen P, and Lappalainen P (2006). Stress fibers are generated by two distinct actin assembly mechanisms in motile cells. J. Cell Biol 173, 383–394. [PubMed: 16651381]
16. Tojkander S, Gateva G, and Lappalainen P (2012). Actin stress fibers– assembly, dynamics and biological roles. J. Cell Sci 125 , 1855–1864. [PubMed: 22544950]
17. Cooper JA, and Schafer DA (2000). Control of actin assembly and disassembly at filament ends. Curr. Opin. Cell Biol 12, 97–103. [PubMed: 10679358]

18. Rao JN, Madasu Y, and Dominguez R (2014). Mechanism of actin fila- ment pointed-end capping by tropomodulin. Science 345 , 463–467. [PubMed: 25061212]
19. Fowler VM, and Dominguez R (2017). Tropomodulins and leiomodins: actin pointed end caps and nucleators in muscles. Biophys. J 112, 1742–1760. [PubMed: 28494946]
20. Parreno J, and Fowler VM (2018). Multifunctional roles of tropomodu- lin-3 in regulating actin dynamics. Biophys. Rev 10 , 1605–1615. [PubMed: 30430457]
21. Fischer RS, Yarmola EG, Weber KL, Speicher KD, Speicher DW, Bubb MR, and Fowler VM (2006). Tropomodulin 3 binds to actin monomers. J. Biol. Chem 281, 36454–36465. [PubMed: 17012745]
22. Fritz-Six KL, Cox PR, Fischer RS, Xu B, Gregorio CC, Zoghbi HY, and Fowler VM (2003). Aberrant myofibril assembly in tropomodu- lin1 null mice leads to aborted heart development and embryonic lethality. J. Cell Biol 163, 1033–1044. [PubMed: 14657235]
23. Sui Z, Nowak RB, Sanada C, Halene S, Krause DS, and Fowler VM (2015). Regulation of actin polymerization by tropomodulin-3 controls megakaryocyte actin organization and platelet biogenesis. Blood 126, 520–530. [PubMed: 25964668]
24. Gregorio CC, Weber A, Bondad M, Pennise CR, and Fowler VM (1995). Requirement of pointed-end capping by tropomodulin to maintain actin filament length in embryonic chick cardiac myocytes. Nature 377, 83–86. [PubMed: 7544875]
25. Gokhin DS, Tierney MT, Sui Z, Sacco A, and Fowler VM (2014). Calpain-mediated proteolysis of tropomodulin isoforms leads to thin filament elongation in dystrophic skeletal muscle. Mol. Biol. Cell 25 , 852–865. [PubMed: 24430868]
26. Gokhin DS, Ochala J, Domenighetti AA, and Fowler VM (2016). Tropomodulin 1-directly controls thin filament length in both wild-type and tropomodulin 4-deficient skeletal muscle. J. Cell Sci 129, e1.2.
27. Moyer JD, Nowak RB, Kim NE, Larkin SK, Peters LL, Hartwig J, Kuypers FA, and Fowler VM (2010). Tropomodulin 1-null mice have a mild spherocytic elliptocytosis with appearance of tropomodulin 3 in red blood cells and disruption of the membrane skeleton. Blood 116, 2590–2599. [PubMed: 20585041]
28. Lim CY, Bi X, Wu D, Kim JB, Gunning PW, Hong W, and Han W (2015). Tropomodulin3 is a novel Akt2 effector regulating insulin-stimu- lated GLUT4 exocytosis through cortical actin remodeling. Nat. Commun 6, 5951. [PubMed: 25575350]
29. Jo YJ, Jang WI, Kim NH, and Namgoong S (2016). Tropomodulin-3 is essential in asymmetric division during mouse oocyte maturation. Sci. Rep 6, 29204. [PubMed: 27374327]
30. Cox-Paulson EA, Walck-Shannon E, Lynch AM, Yamashiro S, Zaidel-Bar R, Eno CC, Ono S, and Hardin J (2012). Tropomodulin protects a-catenin-dependent junctional-actin networks under stress dur- ing epithelial morphogenesis. Curr. Biol 22, 1500–1505. [PubMed: 22771044]
31. Fischer RS, Fritz-Six KL, and Fowler VM (2003). Pointed-end capping by tropomodulin3 negatively regulates endothelial cell motility. J. Cell Biol 161, 371–380. [PubMed: 12707310]
32. Hu S, Dasbiswas K, Guo Z, Tee YH, Thiagarajan V, Hersen P, Chew TL, Safran SA, Zaidel-Bar R, and Bershadsky AD (2017). Long-range self-organization of cytoskeletal myosin II filament stacks. Nat. Cell Biol 19, 133–141. [PubMed: 28114270]
33. Soine JRD, Brand CA, Stricker J, Oakes PW, Gardel ML, and Schwarz US (2015). Model-based traction force microscopy reveals dif- ferential tension in cellular actin bundles. PLoS Comput. Biol 11, e1004076. [PubMed: 25748431]
34. Jiu Y, Pera€nen J, Schaible N, Cheng F, Eriksson JE, Krishnan R, and Lappalainen P (2017). Vimentin intermediate filaments control actin stress fiber assembly through GEF-H1 and RhoA. J. Cell Sci 130 , 892–902. [PubMed: 28096473]
35. Meiring JCM, Bryce NS, Wang Y, Taft MH, Manstein DJ, Liu Lau S, Stear J, Hardeman EC, and Gunning PW (2018). Co-polymers of actin and tropomyosin account for a major fraction of the human actin cytoskeleton. Curr. Biol 28, 2331–2337.e5. [PubMed: 29983319]
36. Evangelista M, Pruyne D, Amberg DC, Boone C, and Bretscher A (2002). Formins direct Arp2/3-independent actin filament assembly to polarize cell growth in yeast. Nat. Cell Biol 4, 32–41. [PubMed: 11740490]

37. Alioto SL, Garabedian MV, Bellavance DR, and Goode BL (2016). Tropomyosin and profilin cooperate to promote formin-mediated actin nucleation and drive yeast actin cable assembly. Curr. Biol 26, 3230–3237. [PubMed: 27866892]
38. Nolen BJ, Tomasevic N, Russell A, Pierce DW, Jia Z, McCormick CD, Hartman J, Sakowicz R, and Pollard TD (2009). Characterization of two classes of small molecule inhibitors of Arp2/3 complex. Nature 460 , 1031–1034. [PubMed: 19648907]
39. Svitkina TM, and Borisy GG (1999). Arp2/3 complex and actin depoly- merizing factor/cofilin in dendritic organization and treadmilling of actin filament array in lamellipodia. J. Cell Biol 145 , 1009–1026. [PubMed: 10352018]
40. Nowak RB, Fischer RS, Zoltoski RK, Kuszak JR, and Fowler VM (2009). Tropomodulin1 is required for membrane skeleton organization and hexagonal geometry of fiber cells in the mouse lens. J. Cell Biol 186, 915–928. [PubMed: 19752024]
41. Gokhin DS, Nowak RB, Kim NE, Arnett EE, Chen AC, Sah RL, Clark JI, and Fowler VM (2012). Tmod1 and CP49 synergize to control the fiber cell geometry, transparency, and mechanical stiffness of the mouse lens. PLoS ONE 7, e48734. [PubMed: 23144950]
42. Brayford S, Bryce NS, Schevzov G, Haynes EM, Bear JE, Hardeman EC, and Gunning PW (2016). Tropomyosin promotes lamel- lipodial persistence by collaborating with Arp2/3 at the leading edge. Curr. Biol 26, 1312–1318. [PubMed: 27112294]
43. Charras G, and Yap AS (2018). Tensile forces and mechanotransduc- tion at cell-cell junctions. Curr. Biol 28, R445–R457. [PubMed: 29689229]
44. Caldwell BJ, Lucas C, Kee AJ, Gaus K, Gunning PW, Hardeman EC, Yap AS, and Gomez GA (2014). Tropomyosin isoforms support actomyosin biogenesis to generate contractile tension at the epithelial zonula adherens. Cytoskeleton (Hoboken) 71, 663–676. [PubMed: 25545457]
45. Kee AJ, Chagan J, Chan JY, Bryce NS, Lucas CA, Zeng J, Hook J, Treutlein H, Laybutt DR, Stehn JR, et al. (2018). On-target action of anti-tropomyosin drugs regulates glucose metabolism. Sci. Rep 8, 4604. [PubMed: 29545590]
46. Suzuki T, Kasamatsu A, Miyamoto I, Saito T, Higo M, Endo- Sakamoto Y, Shiiba M, Tanzawa H, and Uzawa K (2016). Overexpression of TMOD1 is associated with enhanced regional lymphnode metastasis in human oral cancer. Int. J. Oncol 48, 607–612. [PubMed: 26718916]
47. Jin C, Chen Z, Shi W, and Lian Q (2019). Tropomodulin 3 promotes liver cancer progression by activating the MAPK/ERK signaling pathway. Oncol. Rep 41, 3060–3068. [PubMed: 30864730]
48. Paul D, Chanukuppa V, Reddy PJ, Taunk K, Adhav R, Srivastava S, Santra MK, and Rapole S (2016). Global proteomic profiling iden- tifies etoposide chemoresistance markers in non-small cell lung carci- noma. J. Proteomics 138, 95–105. [PubMed: 26898345]
49. Jiu Y, Kumari R, Fenix AM, Schaible N, Liu X, Varjosalo M, Krishnan R, Burnette DT, and Lappalainen P (2019). Myosin-18B pro- motes the assembly of myosin II stacks for maturation of contractile acto- myosin bundles. Curr. Biol 29, 81–92.e5. [PubMed: 30581023]
50. Jiu Y, Lehtima€ki J, Tojkander S, Cheng F, Ja€a€linoja H, Liu X, Varjosalo M, Eriksson JE, and Lappalainen P (2015). Bidirectional interplay between vimentin intermediate filaments and contractile actin stress fibers. Cell Rep. 11, 1511–1518. [PubMed: 26027931]
51. Roux KJ, Kim DI, Raida M, and Burke B (2012). A promiscuous biotin ligase fusion protein identifies proximal and interacting proteins in mammalian cells. J. Cell Biol 196, 801–810. [PubMed: 22412018]
52. Ran FA, Hsu PD, Wright J, Agarwala V, Scott DA, and Zhang F (2013). Genome engineering using the CRISPR-Cas9 system. Nat. Protoc 8, 2281–2308. [PubMed: 24157548]
53. Schneider CA, Rasband WS, and Eliceiri KW (2012). NIH Image to ImageJ: 25 years of image analysis. Nat. Methods 9, 671–675. [PubMed: 22930834]
54. Schevzov G,Whittaker SP,Fath T,Lin JJ,andGunning PW(2011). Tropomyosin isoforms and reagents. Bioarchitecture 1, 135–164. [PubMed: 22069507]
55. Butler JP, Tolic-Nørrelykke IM, Fabry B, and Fredberg JJ (2002). Traction fields, moments, and strain energy that cells exert on their surroundings. Am. J. Physiol. Cell Physiol 282, C595–C605. [PubMed: 11832345]

56. Krishnan R, Park CY, Lin YC, Mead J, Jaspers RT, Trepat X, Lenormand G, Tambe D, Smolensky AV, Knoll AH, et al. (2009). Reinforcement versus fluidization in cytoskeletal mechanoresponsiveness. PLoS ONE 4, e5486. [PubMed: 19424501]

57. Ye J, Coulouris G, Zaretskaya I, Cutcutache I, Rozen S, and Madden TL (2012). Primer-BLAST: a tool to design target-specific primers for polymerase chain reaction. BMC Bioinformatics 13, 134. [PubMed: 22708584]

58. Pardee JD, Simpson PA, Stryer L, and Spudich JA (1982). Actin fil- aments undergo limited subunit exchange in physiological salt conditions. J. Cell Biol 94, 316–324. [PubMed: 7202009]

59. Smillie LB (1982). Preparation and identification of a- and b-tropomyo- sins. Methods Enzymol. 85 , 234–241. [PubMed: 6289041]

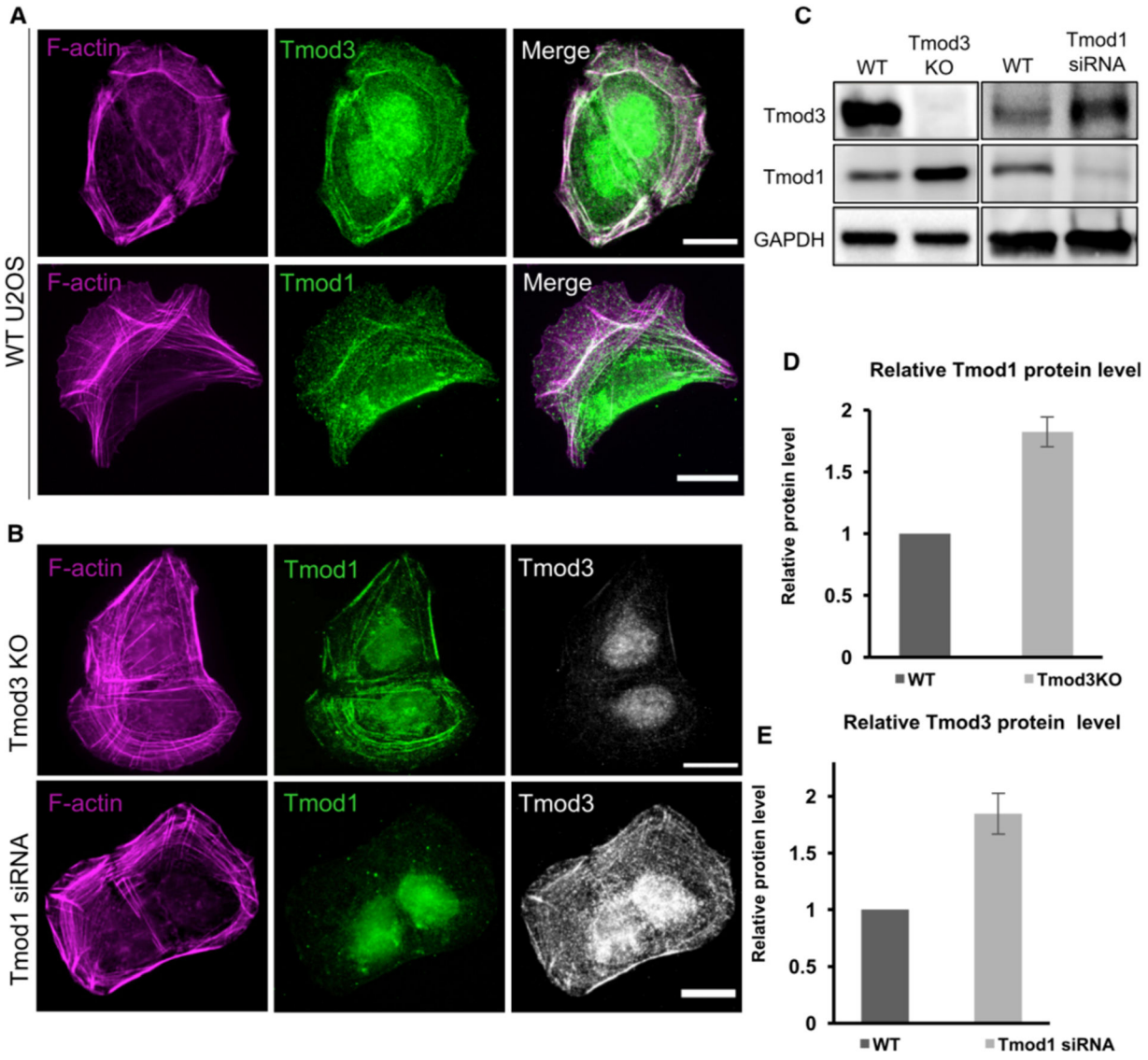

Figure 1. Tmod1 and Tmod3 Are Components of Contractile Actin Stress Fibers

(A) Immunofluorescence images of U2OS cells, where the localization of endogenous Tmod3 and Tmod1 were detected by antibodies and F-actin by phalloidin. Scale bars, 20 mm.

(B) Localization of endogenous Tmod1 and Tmod3 in Tmod3 knockout cells (top) and Tmod1 siRNA cells (bottom). Scale bars, 20 mm.

(C) Western blot analysis of Tmod3 and Tmod1 levels in lysates of wild-type (WT), Tmod3 knockout (Tmod3 KO), and Tmod1 siRNA U2OS cells. GAPDH was probed for equal sample loading.

(D) Relative protein level of Tmod1, quantified by western blot from WT and Tmod3 KO cell lysates. The Tmod1 level in wild-type cells was set to 1, and the data are presented as mean ± SEM; n = 3 for WT and Tmod3 KO total cell lysates.

(E) Relative protein level of Tmod3 in WT and Tmod 1 siRNA cell lysates. The Tmod3 level in wild-type was set to 1, and the data are presented as mean ± SEM; n = 3 for wild-

type and Tmod1 siRNA total cell lysates. Please note that depletion of either Tmod isoform resulted in upregulation of the other one. See also Figure S1 and Table S1.

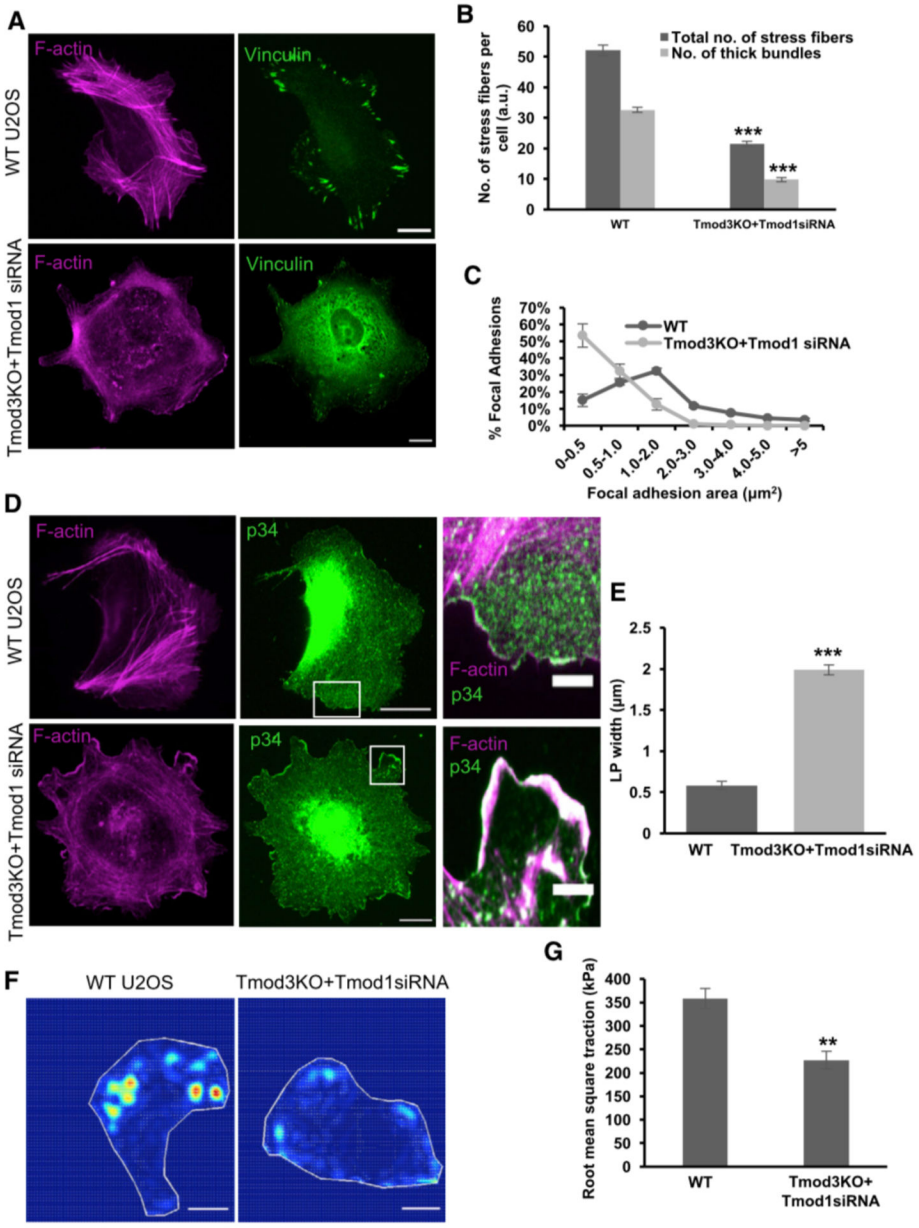

Figure 2. Simultaneous Depletion of Tmod1 and Tmod3 Results in Disruption of Stress Fibers, Increased Lamellipodia Width, and Impaired Force Generation

(A) Distribution of F-actin structures (detected by phalloidin) and focal adhesions (detected by vinculin antibody) in wild-type and Tmod3 KO + Tmod1 siRNA U2OS cells. Scale bars, 20 mm.

(B) Stress fiber analysis of wild-type and Tmod3 KO + Tmod1 siRNA U2OS cells. Data are shown as mean ± SEM; n (cells) = 78 wild-type; n = 67 Tmod3 KO + Tmod1 siRNA. The values obtained from Tmod3 KO + Tmod1 siRNA cells were compared to the ones from wild-type cells. ***p < 0.001 (Stu- dent's t test).

(C) Quantification of the size distributions of focal adhesions. Data are shown as mean ± SEM; n (cells) = 76 wild-type; n = 68 Tmod3 KO + Tmod1 siRNA.

(D) Representative images of wild-type and Tmod3 KO + Tmod1 siRNA U2OS cells, where F-actin was detected by phalloidin and Arp2/3 complex by p34 antibody. Scale bars, 20 mm. Magnified regions of cell edges (corresponding to the white boxes) on the right show examples of F-actin and Arp2/3-rich protrusions in wild-type and Tmod3 KO + Tmod1 siRNA cells. Scale bars, 5 mm.

(E) Quantification of widths of Arp2/3-rich lamellipodial protrusions of wild-type and Tmod3 KO + Tmod1 siRNA U2OS cells. Data are shown as mean ± SEM; n (cells) = 80 wild-type; n = 67 Tmod3 KO + Tmod1 siRNA. ***$p < 0.001$ (Student's t test). (F) Force maps of representative wild-type and Tmod3 KO + Tmod1 siRNA U2OS cells grown on 26 kPa polyacrylamide dishes with fluorescent nanobeads.

(G) Quantification of traction forces in wild-type and Tmod3 KO + Tmod1 siRNA cells. The data are presented as mean ± SEM; n = 41 for both wild- type and 43 for Tmod3 knockout + Tmod1 siRNA cells. **$p < 0.02$ (Student's t test).

See also Figure S2.

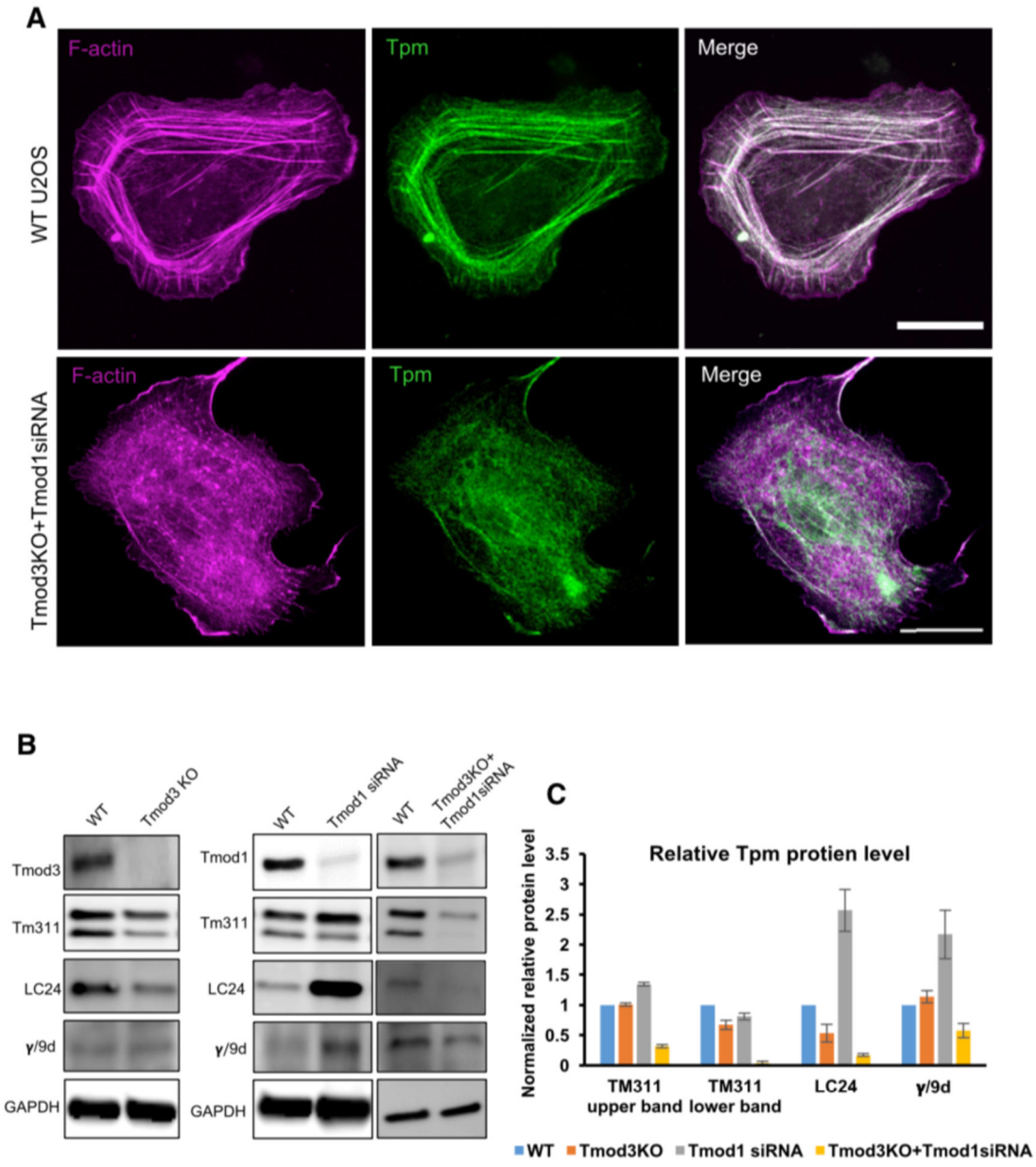

Figure3. SimultaneousDepletionofTmod1 and Tmod3 Leads to a Loss of Tropomyosin-Decorated Actin Filaments

(A) Representative immunofluorescence images of wild-type and Tmod3 KO + Tmod1 siRNA U2OS cells, where F-actin and tropomyosins (Tpm 2.1 and Tmp4.2) were detected by phalloidin and LC24 antibody, respectively. Scale bars, 20 mm. (B) Western blot analysis of Tpm1.6/1.7/2.1 (detected by TM311 antibody), Tpm2.1/4.2 (detected by LC24 antibody), and Tpm3.1/3.2 (detected by g/9d antibody) in lysates of wild-type, Tmod3 KO, Tmod1 siRNA, and Tmod3 KO + Tmod1 siRNA cells. GAPDH was probed for equal sample loading.

(C) Relative protein levels of tropomyosins quantified from wild-type, Tmod3 KO, Tmod1 siRNA, and Tmod3 KO + Tmod1 siRNA U2OS cell lysates. The protein levels in wild-type

cells were set to 1. The data are presented as mean ± SEM; n = 3 for wild-type, Tmod3 KO, Tmod1 siRNA, and Tmod3 KO + Tmod1 siRNA U2OS cells.
See also Figure S3.

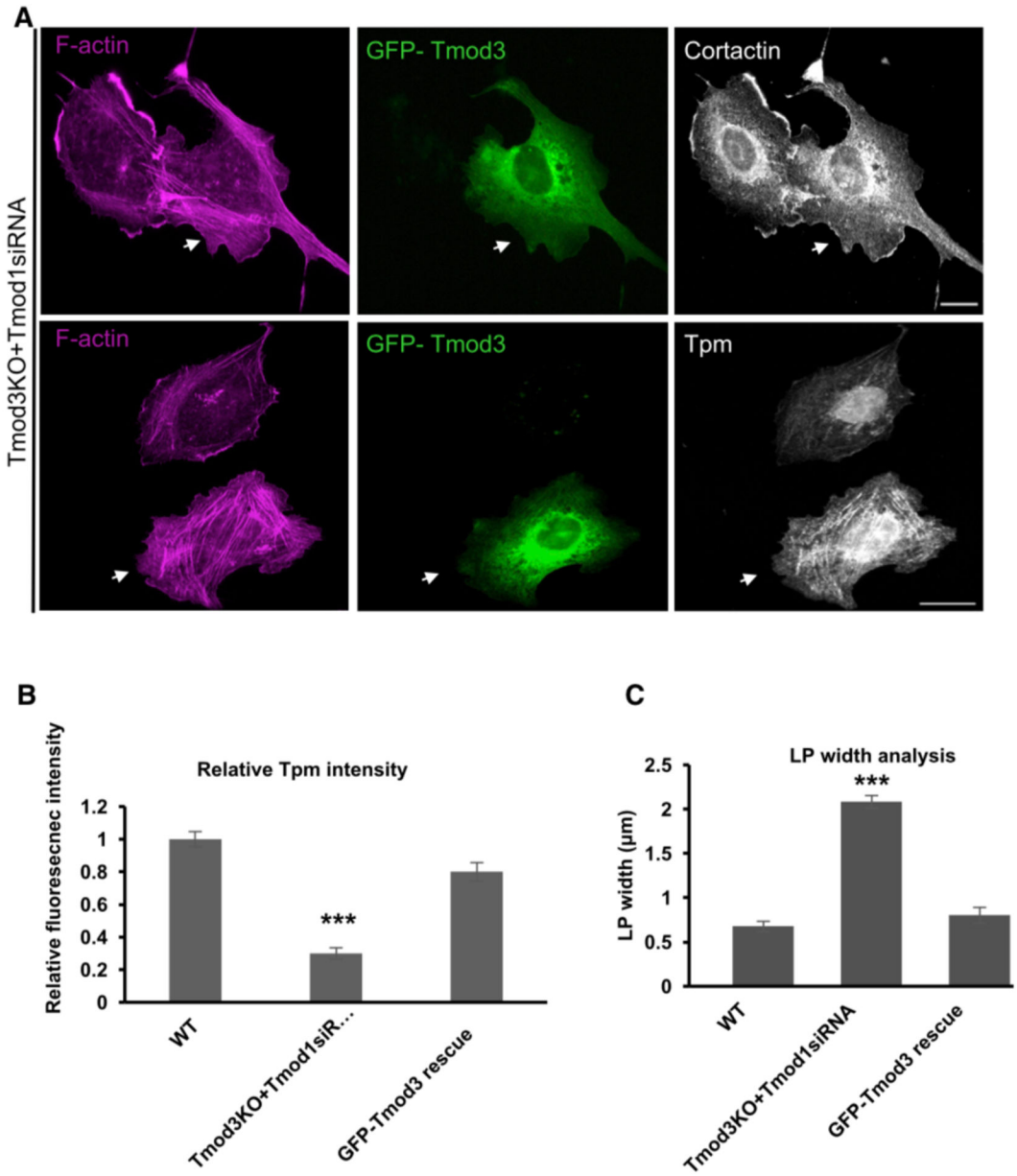

Figure 4. Diminished Tropomyosin Levels and Excessive Lamellipodia Formation, Induced by the Depletion of Tmods, Can Be Rescued by Expression of GFP-Tmod3

(A) Representative examples of Tmod3 KO + Tmod1 siRNA cells expressing GFP-Tmod3. F-actin was visualized by phalloidin, lamellipodia by cortactin antibodies, and Tpm2.1/4.2 by LC24 antibody. The Tmod3 KO + Tmod1 siRNA cells expressing GFP-Tmod3 are highlighted with white arrows. Scale bars, 20 mm.

(B) Normalized relative total fluorescence intensities of Tpm2.1/4.2 (detected by LC24 antibody) quantified from immunofluorescence images of un- transfected and GFP-Tmod3 expressing Tmod3 KO + Tmod1 siRNA cells from the same image and the wild-type cells from a different set of images from an identical experiment. The values of wild- type cells were set to 1, and the data are presented as mean ± SEM; n = 58 wild-type cells; n = 46 cells from 21 images for both untransfected Tmod3 KO + Tmod1 siRNA cells and GFP-Tmod3

expressing Tmod3 KO + Tmod1 cells. The values obtained from the knockout and rescue cells were compared to the ones from wild-type cells. ***p < 0.001 (Stu- dent's t test). (C) Analysis of lamellipodia widths quantified from Arp2/3 immunofluorescence images of wild-type, Tmod3 KO + Tmod1 siRNA, and GFP-Tmod3 rescue cells. Data are presented as mean ± SEM; n = 67 wild-type; n = 58 Tmod3 KO + Tmod1 siRNA cells; n = 48 GFP-Tmod3 rescue cells. The values obtained from knockout and rescue cells were compared to the ones from wild-type cells. ***p < 0.001 (Student's t test).

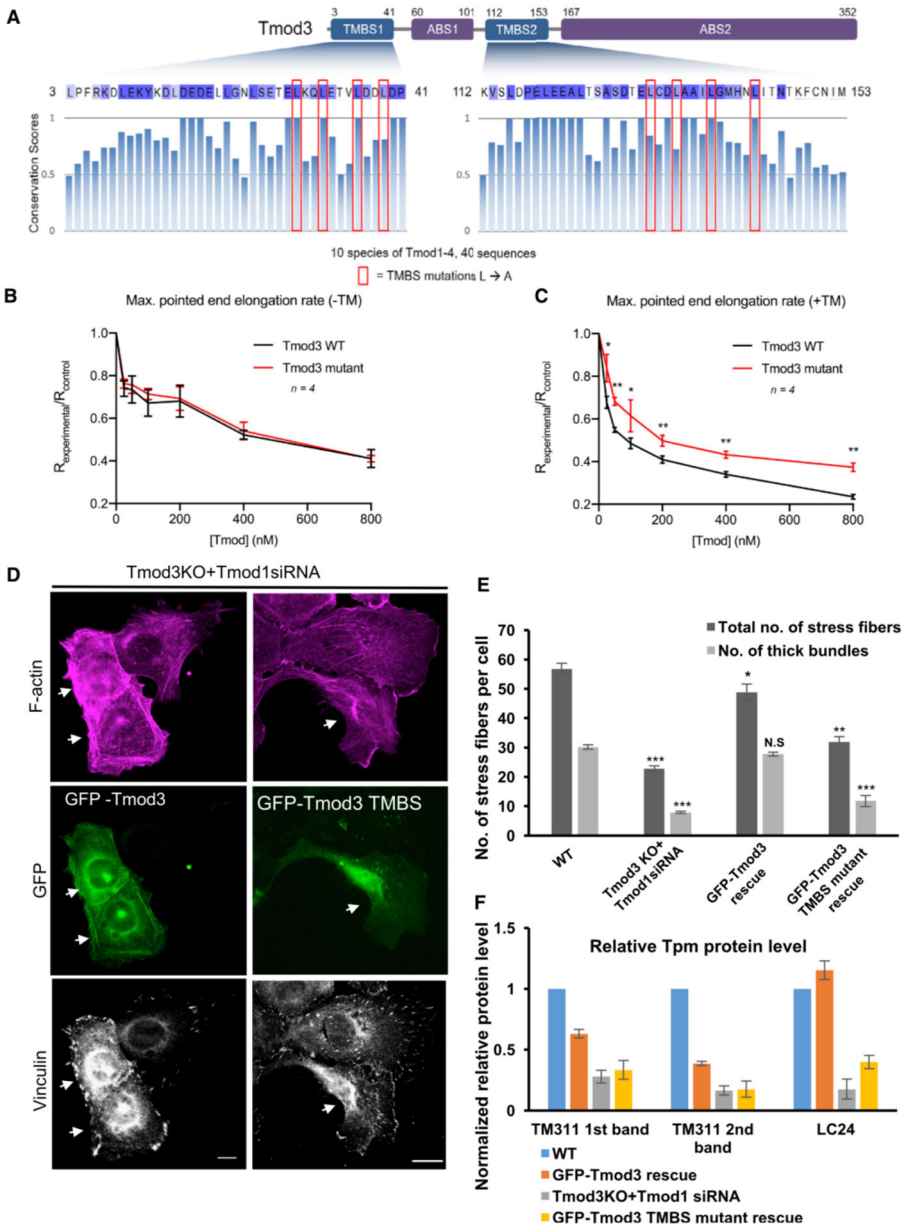

Figure 5. The Tropomyosin-Binding Sites (TMBSs) of Tmod3 Are Critical for Its Function In Vitro and in Cells

(A) Sequences of tropomyosin-binding sites 1 (TMBS1) and 2 (TMBS2) from human tropomodulin-3, colored by conservation score. Red boxes highlight the conserved leucine residues that were mutated to ablate tropomyosin binding.

(B and C) Maximum polymerization rates (normalized to 0 nM Tmod control) of 1.5 mM (6% pyrene labeled) actin in the presence of 1.5 mM F-actin seeds, 25 nM CapZ, and various concentrations of either WT or TMBS mutant Tmod3 in the absence (B) or presence (C) of 1 mM tropomyosin. Each point represents mean ± SEM; n = 4 elongation curves. One star (*) indicates that zero difference in means fell outside the 95% credible interval; two stars (**) indicate that zero difference in means fell outside the 99% credible interval.

(D) Representative images of Tmod3 KO + Tmod1 siRNA cells expressing GFP-Tmod3 (left) or GFP-Tmod3 TMBS mutant (right). F-actin was visualized by phalloidin and focal adhesions by vinculin antibody. White arrows highlight the cells expressing GFP-Tmod3 constructs. Scale bars, 20 mm.

(E) Stress fiber analysis (by Ridge detection plugin of Fiji ImageJ) from wild-type, Tmod3 KO + Tmod1 siRNA, GFP-Tmod3 rescued, and GFP-Tmod3 TMBS mutant rescued cells. Data are shown as mean ± SEM; n (cells) = 79 wild-type; n = 71 Tmod3 KO + Tmod1 siRNA; n = 48 GFP-Tmod3 rescue; n = 45 GFP-Tmod3 TMBS mutant rescue. The values obtained from knockout/knockdown and rescue cells were compared to the ones from wild-type cells. N.S. (not significant); *$p < 0.05$; **$p < 0.02$; ***$p < 0.001$ (Student's t test).

(F) Relative protein levels of tropomyosins quantified from wild-type, GFP-Tmod3 rescue, Tmod3 KO + Tmod1 siRNA, and GFP-Tmod3 TMBS mutant rescue U2OS cell lysates. The protein levels in wild-type cells were set to 1. The data are presented as mean ± SEM; n = 3 for wild-type, GFP-Tmod3 rescue, Tmod3 KO + Tmod1 siRNA, and GFP-Tmod3 TMBS mutant rescue U2OS cells.

See also Figures S4 and S5.

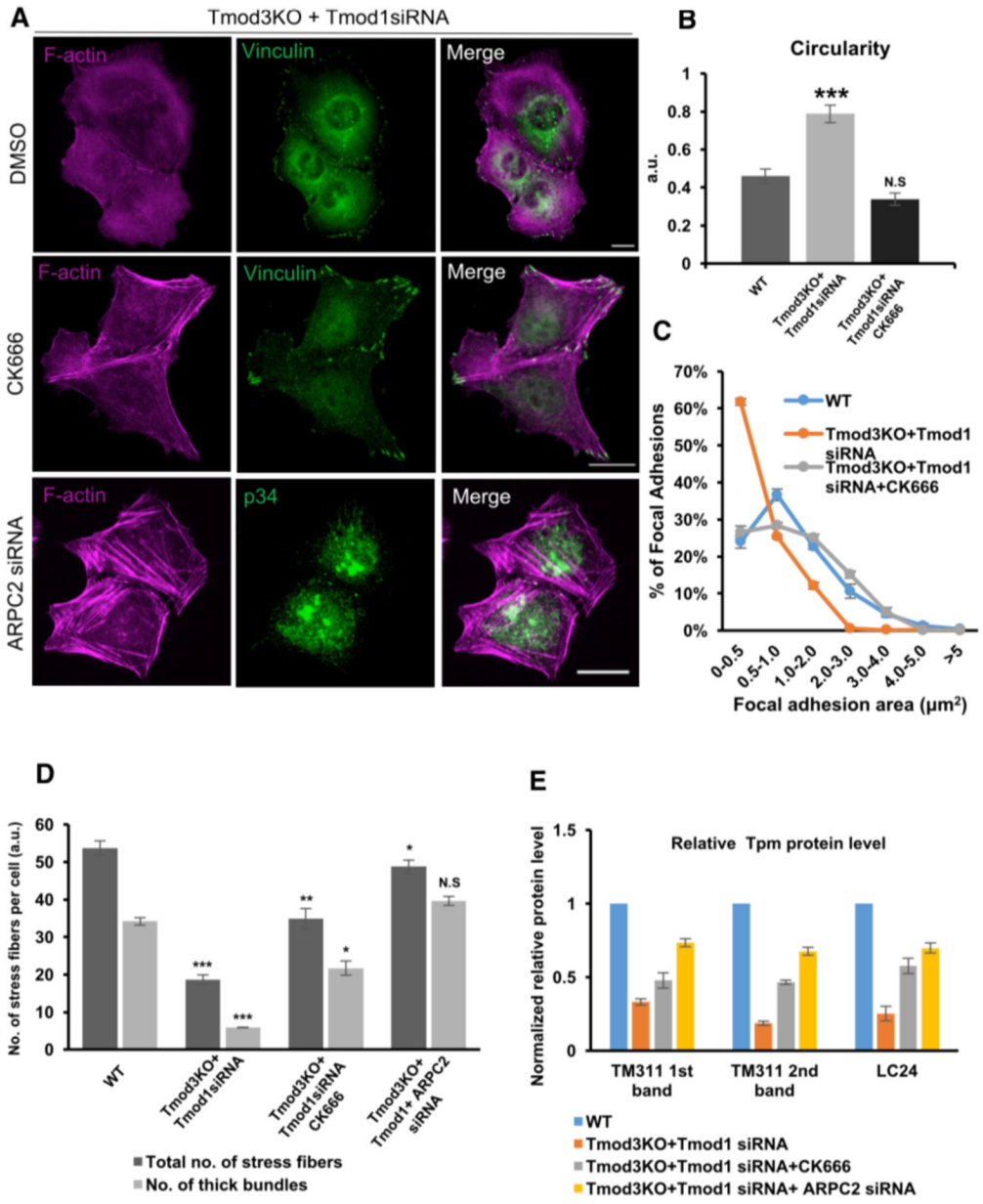

Figure6. TmodsAntagonizewiththe Arp2/3 Complex in Stabilizing Tropomyosin-Deco- rated Actin Stress Fibers

(A) Representative examples of Tmod3 KO + Tmod1 siRNA cells treated with DMSO or 100 mM CK666 or in which the ARPC2 subunit of the Arp2/3 complex was depleted by siRNA. F-actin was detected by phalloidin and focal adhesions and Arp2/3 complex by vinculin and p34 antibodies, respectively. Scale bars, 20 mm. Please note the re-appearance of stress fibers and an increase in the size of focal adhesions in Tmod knockout/knockdown cells after treatment with the Arp2/3 complex inhibitor or following siRNA depletion of the functional Arp2/3 complex.

(B) Analysis of cell circularity index of wild-type cells, Tmod3 KO + Tmod1 siRNA cells, and Tmod3 KO + Tmod1 siRNA treated with CK666. The values obtained from untreated and CK666-treated knockout/ knockdown cells were compared to the ones from wild-type

cells, and the data are shown as mean ± SEM; n (cells) = 80 wild-type; n = 72 Tmod3 KO + Tmod1 siRNA; n = 72 Tmod3 KO + Tmod1 siRNA + CK666. ***p < 0.001 (Student's t test).

(C) Size distributions of focal adhesions in wild- type cells, Tmod3 KO + Tmod1 siRNA cells, and CK666-treated Tmod3 KO + Tmod1 siRNA cells. Data were obtained and analyzed as in Figure 2C and presented as mean ± SEM; n (cells) = 62 wild- type; n = 64 Tmod3 KO + Tmod1 siRNA; n = 67 Tmod3 KO + Tmod1 siRNA + CK666.

(D) Stress fibers analysis (by Ridge detection plugin of Fiji ImageJ) from wild-type cells, Tmod3 KO + Tmod1 siRNA cells, CK666-treated Tmod3 KO + Tmod1 siRNA cells, and ARPC2 siRNA + Tmod3 KO + Tmod1 siRNA cells. Data are shown as mean ± SEM. The values obtained from un- treated, CK666-treated, and ARPC2 depleted knockout/ knockdown cells were compared to the ones from wild-type cells. n (cells) = 73 wild-type; n = 69 Tmod3 KO + Tmod1 siRNA; n = 58 Tmod3 KO + Tmod1 siRNA + CK666; n = 55 Tmod3 KO + Tmod1 siRNA + ARPC2 siRNA. *p < 0.05; **p < 0.02; ***p < 0.001 (Student's t test).

(E) Relative protein levels of tropomyosins quantified from wild-type, Tmod3 KO + Tmod1 siRNA, CK666-treated Tmod3 KO + Tmod1 siRNA cells, and ARPC2 siRNA + Tmod3 KO + Tmod1 siRNA U2OS cell lysates. The protein levels in wild-type cells were set to 1. The data are presented as mean ± SEM; n = 3 for wild- type, Tmod3 KO + Tmod1 siRNA, CK666-treated Tmod3 KO + Tmod1 siRNA cells, and ARPC2 siRNA + Tmod3 KO + Tmod1 siRNA U2OS cells.

See also Figure S6.

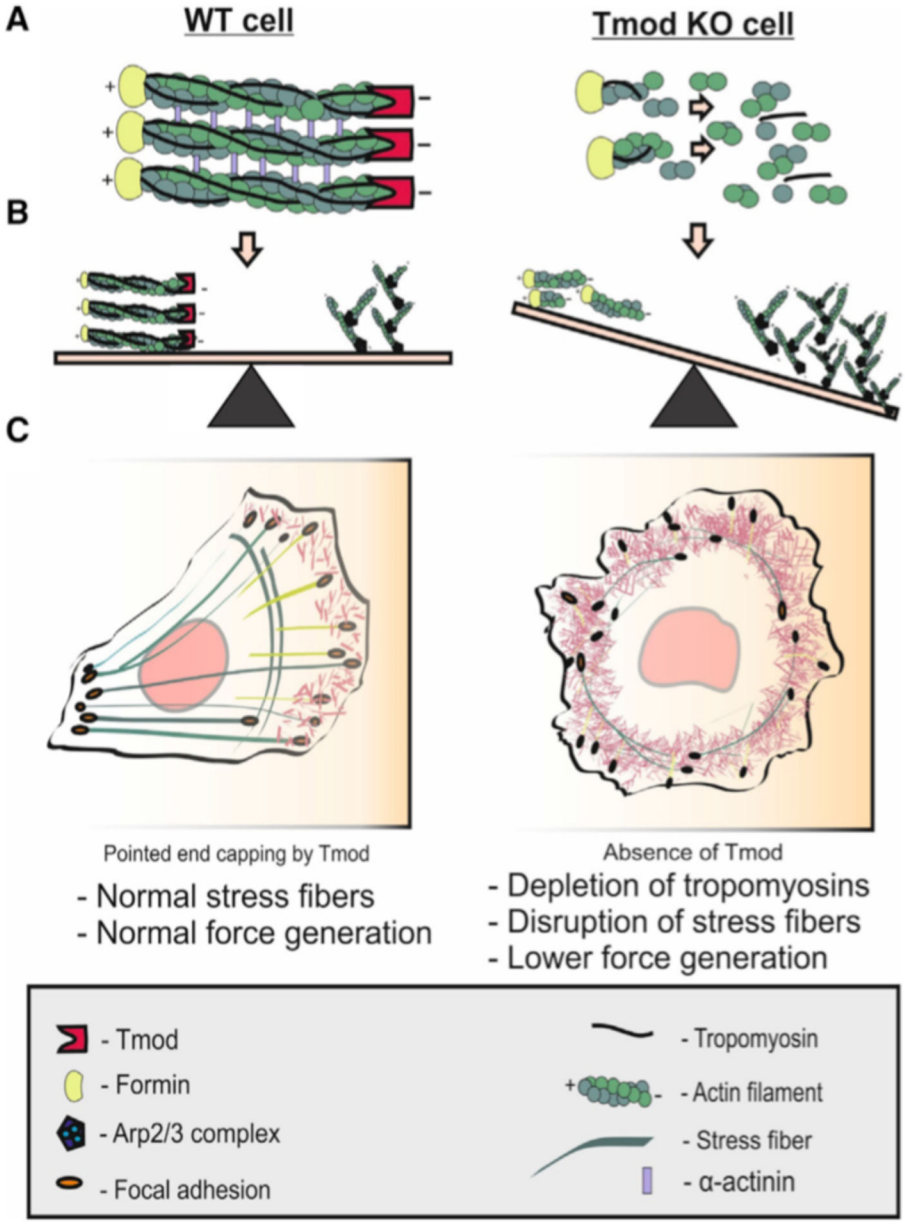

Figure 7. A Working Model for the Role of Tmods in Stabilizing Tropomyosin-Actin Filaments and Hence Maintaining the Homeo- stasis between Arp2/3-Complex-Nucleated Protrusive and Tropomyosin-Decorated Contractile Actin Filament Pools in Cells

(A) Actin filaments that are polymerized by formins and decorated by tropomyosins are stabilized through pointed-end capping by Tmods (left). In the absence of Tmods, these filaments become unstable (right).

(B) Depletion of Tmods results in disruption of tropomyosin-decorated actin filaments and consequent increase in the Arp2/3-nucleated actin filament networks.

(C) This unbalance in actin filament homeostasis results in the loss of stress fibers and consequent decrease in force generation.